SCIENCE CHINA Materials ARTICLES

mater.scichina.com link.springer.com

Published online 17 January 2018 | https://doi.org/10.1007/s40843-017-9183-2

Sci China Mater 2018, 61(6): 869–877

SPECIAL ISSUE: Advanced Materials for Photoelectrochemical Cells

A simple green approach to synthesis of sub-100 nm carbon spheres as template for TiO_2 hollow nanospheres with enhanced photocatalytic activities

Yubo Tan[1], Maochang Liu[1], Daixing Wei[1], Heming Tang[2], Xinjian Feng[2*] and Shaohua Shen[1*]

ABSTRACT **Carbon spheres (CSs) have attracted great attention given their wide applications in bio-diagnostics, photonic band-gap crystals and drug delivery, etc. The morphology and size of CSs greatly affect their performances and applications. Herein, we report a green and catalyst-free hydrothermal carbonization (HTC) method to synthesize CSs with glucose as carbon precursor. The diameter of CSs can be tuned within a wide range from 450 to 40 nm by controlling the glucose concentration, reaction time and temperature. Using the obtained CSs as template, hollow TiO_2 nanospheres (HTNSs) with controllable diameters are prepared *via* a sol-gel method. As photocatalysts for hydrogen generation, the photoactivity of the HTNSs shows strong dependence upon size, and is much higher than that of solid TiO_2. With particle size decreasing, the photoactivity of the obtained HTNSs gradually increases. Without any co-catalyst, the highest photocatalytic hydrogen generation activity is obtained with HTNSs of 40 nm in diameter, which exceeds that of solid TiO_2 and commercial P25 by 64 times and 3 times, respectively.**

Keywords: carbon nanospheres, hydrothermal carbonization, hollow titanium dioxide nanospheres, photocatalytic hydrogen production

INTRODUCTION

Titanium dioxide (TiO_2) is one of the most important photocatalytic materials because of its nontoxicity, low-cost, and good chemical stability [1,2]. Compared with their solid counterparts, hollow TiO_2 nanoparticles (NPs) with porous walls have been intensively explored due to their enlarged surface areas, reduced densities and enhanced photocatalytic activity [3–7]. Considerable efforts have been made in preparing TiO_2 hollow nanostructures [7–11]. For the fabrication of TiO_2 shells, different templating approaches using hard or soft templates [8,12–14], layer-by-layer coating or emulsion/interfacial polymerization [15,16] have been successfully demonstrated in past years. In comparison to organic surfactants as soft templates, hard templates (such as polymer microspheres [7], metal (Au, Ag, Pt) colloid beads [5,17,18], and silica spheres) could generate hollow TiO_2 nanostructures [19] with controllable monodispersity and size. However, the hard templating methods mentioned above usually inevitably introduce different organic reagents serving as surfactants or catalysts, and strong oxidative reagents for precious metal corrosion. These drawbacks not only lead to high cost, but also limit the subsequent biological application .

Colloidal carbon spheres (CSs), which have widely functioned as catalyst support, adsorbent, anode materials and biological medicine, etc. [20–26], could also serve as a hard template for the synthesis of hollow nanostructures [14,25]. Various techniques including hydrothermal carbonization (HTC) [26], chemical vapor deposition [27], ultrasonic-spray [28], and catalytic pyrolysis of polymers [29,30], have been applied to synthesize CSs with tunable diameters ranging from nanometers to micrometers. Among these approaches, HTC method is the most versatile one, for its relatively low reaction temperature and facile synthesis procedure. Notably, the hydrothermally synthesized CSs always possess lots of oxygen-containing functional groups, avoiding subsequent surface mod-

[1] International Research Center for Renewable Energy, State Key Laboratory of Multiphase Flow in Power Engineering, Xi'an Jiaotong University, Xi'an 710049, China

[2] College of Chemistry, Chemical Engineering and Materials Science, Soochow University, Suzhou 215123, China

* Corresponding authors (emails: shshen_xjtu@mail.xjtu.edu.cn (Shen S); xjfeng@suda.edu.cn (Feng X))

ifications when used as template. In 2001, Wang *et al.* [31] firstly documented the HTC synthesis of nanosized CSs, with diameters ranging from 250 nm to 5 μm. Later in 2004, Sun *et al.* [32] synthesized micro-scale CSs by using glucose as carbon precursor. More endeavours were then donated to using glucose as carbon precursor to fabricate structure and size tailored CSs *via* the HTC process, with the assistance of surfactants (polyvinyl alcohol, polyethylene glycol, ethylenediamine, etc.), catalysts (inorganic acid, alkalis, metallic oxides, metal salts), and even both (Table S1). These essential organic or inorganic additives inevitably introduced impurities in the CSs. Moreover, the report on the HTC synthesis of CSs with diameter below 100 nm is still rare, primarily due to the ineffective capping ability of surfactant (Table S1). These aforementioned limitations greatly restrict the controllable and facile synthesis of small-sized (e.g., sub −100 nm) CSs and their applications in different fields of energy storage, drug delivery, sensors and hard templates for the synthesis of hollow structure with small and controllable size.

Herein, we demonstrated a green and catalyst-free HTC method for the fabrication of CSs, with the only carbon precursor, glucose. By varying parameters including glucose concentration, pH value, reaction time and temperature, the diameters of the obtained CSs could be tailored from 40 to 450 nm. The as-prepared CSs were then used as sacrificial templates to synthesize hollow TiO_2 nanospheres (HTNSs) in different sizes (40, 140, 450 nm), as photocatalysts for photocatalytic H_2 evolution from aqueous solution without loading any noble metal as co-catalyst. It was found that the photoactivity of HTNSs was size dependent, and the highest photocatalytic activity achieved by 40 nm HTNSs could exceed 3 folds that of the benchmarking commercial P25 TiO_2. This study offers a facile and green HTC route to prepare sub−100 nm CSs and HTNSs, which could also be used to synthesize other semiconductor nanocrystals possessing hollow structures.

EXPERIMENTAL SECTION

Preparation of CSs

CSs with tuneable sizes were fabricated through a HTC method. In a typical synthesis, glucose (1–20 g, ≥ 99.5%, Sinopharm Chemical Reagent Co., Ltd.) was dissolved in (100 mL) distilled water to form a clear solution. The pH value was adjusted from 2.5 to 12.5 by adding ammonium hydroxide ($NH_3{\cdot}H_2O$, 25.0%–28.0%, Sinopharm Chemical Reagent Co., Ltd.) or hydrochloric acid (HCl, 36.5%–38.0%, ca. 12 mol L^{-1}, Sinopharm Chemical Reagent Co., Ltd.). 10 mL of the obtained solution was transferred into a Teflon-sealed autoclave (25 mL) and maintained at a desired temperature (180–200°C) for a certain time (2–8 h). The autoclave then was cooled down to room temperature naturally. The as-synthesized products were separated by centrifugation, purified by several cycles of centrifugation/washing/redispersion in water and ethanol (≥ 99.5%, Sinopharm Chemical Reagent Co., Ltd.), until the solution turned clear. Finally, the products were dried in an oven at 80°C for more than 8 h. The detailed experimental recipes were listed in Table S2. Herein, a typical process for the synthesis of CSs was defined by keeping the concentration of CSs at 0.08 g mL^{-1}, 180°C, for 4 h, and pH value at 6.5.

Preparation of HTNSs

HTNSs were synthesized by a sol-gel method. In a typical synthesis, 20 mg of CSs (40, 140, 450 nm) and 150 μL of water were added into 48 mL of ethanol, and ultrasonicated until uniform dispersion. With continuous stirring, 120 μL of tetra-*n*-butyl titanate (TBOT, ≥ 98.0%, Sinopharm Chemical Reagent Co., Ltd.) was added in the above mixed solution and kept at 60°C for 2 h. After centrifugation, the products were dried at 50°C for 12 h in an oven and the CSs/TiO_2 core-shell structures were then obtained. HTNSs were prepared by an oxidation etching, i.e., the CSs/TiO_2 core-shell structures were calcinated at 550°C (heating rate: 2°C min^{-1}) for 3 h in a muffle furnace under air condition. Solid TiO_2 particles were synthesized *via* the same procedure without CSs as template.

Characterization

The morphology and structure of the as-prepared CSs was investigated by a field emission scanning electron microscope (FESEM, S4800, Hitachi, Tokyo, Japan) at an accelerating voltage of 5 kV and a transmission electron microscope (TEM, F20, FEI, Hillsboro, USA) operated at 200 kV. The size distribution of the as-synthesized CSs was determined based upon direct measurement over 50–100 NPs in the FESEM images. The thermal stability of CSs was characterized by a thermogravimetric analyser (TGA, TGA-7, PE, USA) with a heating rate of 10°C min^{-1}, under oxygen/nitrogen flow. The crystallinity of the samples was analyzed by X-ray diffraction (XRD, X'Pert PRO MPD, PANalytical, Netherlands) performed on a Rigaku diffractometer (40 kV, 40 mA; Cu Kα radiation, λ = 1.541874 Å; Ni filter; real time multiple strip (RTMS) detector, X'Celerator) with 2θ varied from 20° to

80°. Surface functional groups were measured on a Fourier transform infrared spectroscope (FTIR, Vetex 70, Bruker, Germany) with dry-pressed tableting samples at room temperature. The charge carrier behaviour was investigated on a surface photovoltage (SPV) spectroscope (PL-SPS1000, Perfectlight Ltd., Beijing, China).

Photocatalytic activity evaluation

The photocatalytic hydrogen evolution was carried out in a gas-closed system. Specifically, a 115 mL Pyrex cell with a flat and round-side window to external light incidence was employed as the photo-reactor. A 300 W Xe arc lamp (PLS-SXE300, Beijing Trusttech Technology Co., Ltd, China) was used as the light source. Photocatalytic reaction temperature was kept at 35°C controlled by thermostatic circulating water. Hydrogen gas was detected by a gas chromatograph (GC, SP-2100, Beijing Beifen-Ruili Analytical Instrument Co., Ltd, China) equipped with a TDX-01 column, thermal conductivity detector (TCD), with N_2 as carrier-gas. In a typical photocatalytic experiment, 8 mg of the photocatalyst powder was dispersed into 80 mL aqueous solution containing 7.5 mL of triethanolamine (TEA, ≥ 99.5%, Sinopharm Chemical Reagent Co., Ltd.) as sacrificial agent to eliminate photogenerated holes. The suspension was degased by N_2 for 20 min to remove oxygen before photocatalytic reaction. Commercial P25 (Evonik Degussa) was used as the reference photocatalyst.

RESULTS AND DISCUSSION

Fig. 1a, b are the FESEM and TEM images of nanosized CSs prepared *via* the defined typical process, with glucose concentration of 0.08 g mL^{-1} at 180°C for 4 h, and an initial pH value of 6.5. The CSs have smooth surface, good structural integrity and average diameter of ~80 nm. During the hydrothermal process, the color of the solution turned from transparent to light yellow, brown and finally black, as shown in Fig. S1, indicating that LaMar model should be responsible for the formation of CSs by HTC method using glucose.

Fig. 1c shows the influence of glucose concentrations on the diameters of obtained CSs. With spherical shape well maintained (see FESEM images shown in Fig. S2), the average size of the obtained CSs increased with the increasing glucose concentrations, with the smallest average diameter of 40 nm obtained with glucose concentration of 0.01 g mL^{-1}. Sub-100 nm CSs could be obtained only when the concentration of glucose was less than 0.1 g mL^{-1}. Moreover, from the FESEM images shown in Fig. S2 and the particle sizes listed in Table S2 (see samples S28, S33–S35), lower concentration benefits the narrow size distribution. For example, CSs prepared by 0.01 g mL^{-1} glucose solution possess uniform size distribution, with an average diameter of 40 nm and size deviation of ±5 nm; while the size deviation becomes much wider when the concentration of glucose is increased to 0.16 g mL^{-1}, with average diameter ranging from 140 to 185 nm. It is proposed that higher glucose concentration benefits the formation of 5-hydroxymethylfurfural (HFM) nucleus [26], and then the large amount of HFM nuclei promotes the Ostwald ripening process as well as the nucleation. As a result, with larger particles formed, the increasing nucleation rate decreases the growth synchronicity of seeds into final particles, resulting in size inhomogeneity.

The effect of initial pH on the average size of CSs was also investigated, with size distribution and FESEM images shown in Fig. 1d and Fig. S3, respectively. When the pH varied from 3.5 to 9.5, no significant change in CSs diameters was observed. However, when the pH was higher than 10 or lower than 3, the diameter of CSs dramatically increased to 400–500 nm, with reduced uniformity. This indicates that the pH may be closely related to the reaction rates. Strong acidic/basic condition is conducive to the higher reaction rate, which may accelerate the degradation of glucose and the growth of CSs [33]. Instead, a mild pH condition favours the formation of CSs with size below 100 nm. In addition, surface properties of CSs could be modified in strong acidity or basicity, which will be further discussed in the following FTIR analysis, leading to the change of morphology of CSs.

The influence of reaction temperature and time on the growth of CSs was conducted, with the dependence of the average diameters of CSs on the reaction temperature and time documented in Fig. 1e, f based on the FESEM images in Figs S4, S5. It was observed that with the reaction temperature increasing from 180 to 200°C, the diameters of the CSs gradually increased (Fig. 1e); while at the temperature lower than 180°C, CSs could hardly form during the HTC process, no matter how long the reaction proceeded (Table S2). The asymmetric growth induced by particle attachment happened at higher temperature (>180°C). For instance, as shown in Fig. S4b, c, the CSs stick together and form irregular branches. The effect of reaction time on the growth of CSs cannot be ignored either. As shown in Fig. 1f and Fig. S5, increasing reaction time guaranteed the carbonization of glucose and then the growth of CSs as expected, accompanying the gradual increase in the diameters of CSs. However,

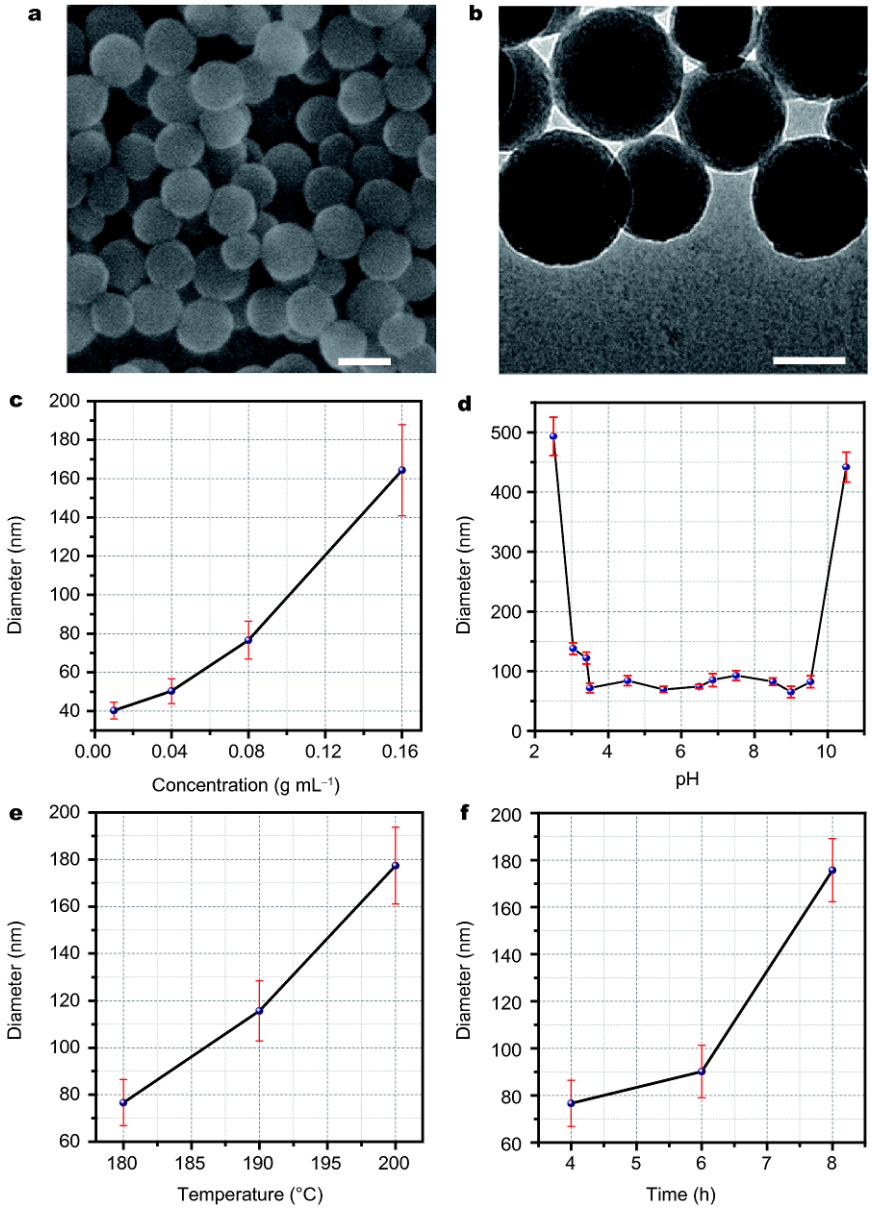

Figure 1 (a, b) Typical FESEM and TEM images of the CSs obtained *via* HTC method. Average diameter of CSs obtained *via* the defined typical synthesis process with (c) glucose concentrations varying from 0.01 to 0.16 g mL^{-1}, (d) pH varying from 2.5 to 10.5, (e) reaction temperatures varying from 180 to 200°C, and (f) reaction times varying from 2 to 8 h. The scale bar in (a) and (b) is 100 nm.

the obtained CSs happened to aggregate when the reaction time was extended to 4 h. For example, with time extending to 8 h, the average diameter of CSs reaches ~175 nm, with serious adhesion between neighbour CSs. This transformation might be due to the slow dehydration of the surface functional groups on CSs [32,33], leading to an automatic bonding between the CSs. These results indicate that there exists critical reaction temperature and reaction time for the formation of CSs with good spherical shape and uniform size upon the HTC of glucose [32].

FTIR analysis was carried out to verify the functional groups involved in the CSs and the conversion of glucose in the HTC process. As shown in Fig. 2a, there are several peaks corresponding to oxygenic groups, including the C–O stretching peaks between 1,000–1,300 cm^{-1}, the C=O stretching vibration peak at 1,726 cm^{-1}, and the vibration and deformation peaks of O–H groups around

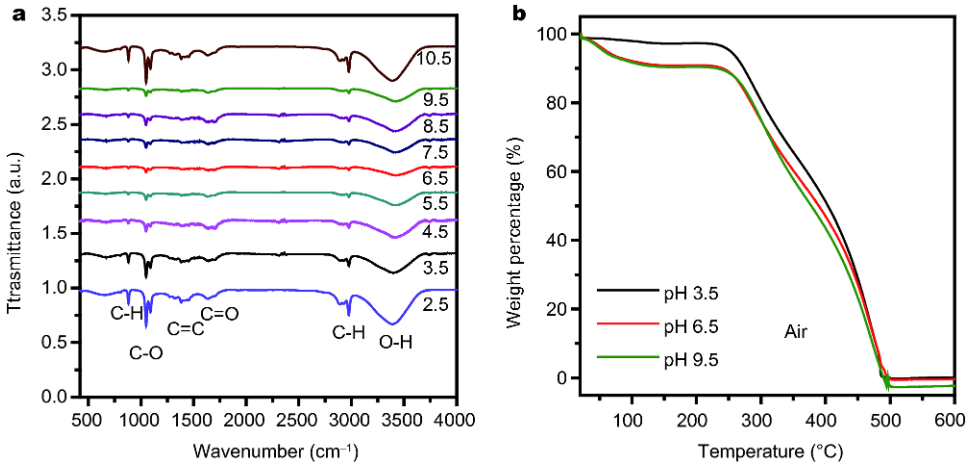

Figure 2 (a) FTIR patterns of the CSs obtained with different initial pH values (from 2.5 to 10.5); concentration: 0.08 g mL^{-1}; reaction time: 4 h; temperature: 180°C. (b) TGA curves of CSs performed in air, heated to 600°C.

3,500 cm^{-1}. Such oxygen-containing functional groups can not only improve the hydrophilicity and stability of the CSs in aqueous systems, but also broaden its application in the fields of biological, diagnostics, and drug delivery, especially as templates for hybrid core/shell structures or hollow/porous materials. The peaks at 890 and 3,000 cm^{-1} resulted from the out-of-plane bending vibration of C–H on *para*-disubstituted rings, indicating the aromatization occurred during hydrothermal treatment. The peaks between 1,450–1,600 cm^{-1} are assigned to typical C=C vibrations, which implies the presence of benzene rings and thus the aromatization of the products. Although the as-prepared CSs synthesized in different initial pH values have the same kind of characteristic peaks, it must be mentioned that when the pH value is <3 or >10, the absorption peaks of C–H are significantly enhanced, consistent with the diameter growth trend of the CSs prepared in strong acidity or basicity (Fig. 1d and Fig. S3). Based on Fig. S1 and the analysis above, one possible reason for the growth of large CSs is that more stable aromatic structures formed *via* aromatization reactions in strong acidity or basicity promote the formation and growth of CSs in large size.

In order to confirm the calcination temperature to burn out CSs for subsequent template application, the as-prepared CSs were further analyzed by TGA. Fig. 2b and Fig. S6 show the TGA curves of the CSs samples obtained at different pH values annealed in oxygen and nitrogen atmosphere, respectively. Obviously, all the obtained CSs display good thermal stability in nitrogen atmosphere, with the morphology kept unchanged even with temperature increased up to 1,000°C (Fig. S6), while the CSs start to degrade at 270°C and are completely burnt out, with the temperature approaching 500°C in air (Fig. 2b). These TGA results provide the experimental guides for the subsequent calcination of CSs/TiO_2 core-shell structures for the controlled synthesis of HTNSs with CSs as hard templates. It is worthwhile mentioning that the CSs could be very stable as the temperature up to 1,000°C in nitrogen atmosphere (Fig. S6), which implied that the as-synthesized CSs may have great potential as high temperature material under special conditions.

These oxygen-containing functional groups enriched CSs were then used as template for the conformal growth of CSs/TiO_2 core-shell structures with controlled sizes. HTNSs were obtained by high-temperature calcination (e.g., 550°C, 3 h) to burn out the core of CSs. Fig. 3a shows a schematic illustration of the formation of CSs/TiO_2 core-shell structure and their subsequent conversion into HTNSs. Fig. 3b–j show the FESEM and TEM images of the CSs in different sizes (40, 140 and 450 nm) as templates, the conformally formed CSs/TiO_2 core-shell structure and the HTNSs with CSs burnt out. Three different sized CSs with perfect spherical shape and uniform size distribution (Fig. 3b, e, h) were employed to control the sizes of the CSs/TiO_2 core-shell structures and then the HTNSs. Fig. 3c, f, i present the FESEM images of the formed HTNSs in different sizes after calcination, which clearly demonstrated the hollow interiors and the porous shells of HTNSs formed by the combustion of CSs. The three different sized HTNSs formed from the corresponding CSs as hard template were also found with good monodispersity in average diameters of ~40 nm (HTNS-40), ~140 nm (HTNS-140) and ~450 nm (HTNS-450), respectively. In comparison, without CSs as templates, irregular TiO_2 spheres with poor size dispersity

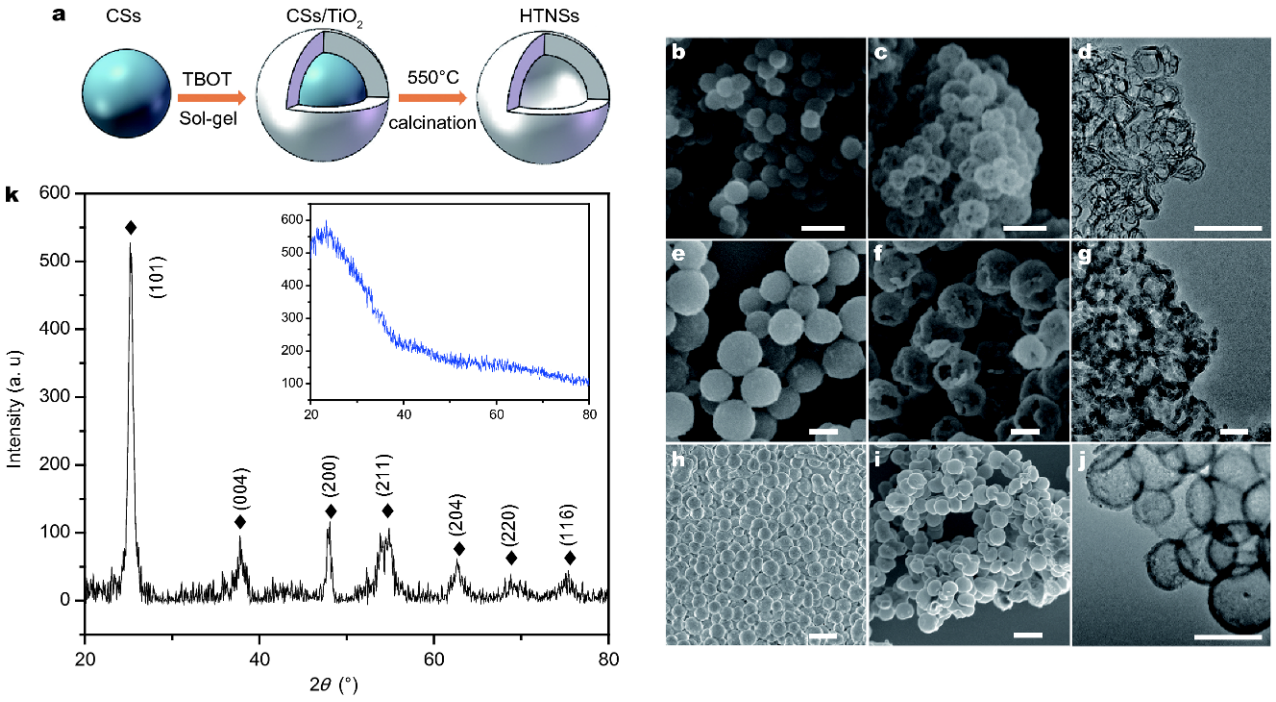

Figure 3 (a) Schematic illustration of the preparation of HTNSs. (b, e and h) FESEM images of CSs with an average size of 40, 140 and 450 nm, respectively. (c, f and i) FESEM images of corresponding HTNSs (HTNS-40, HTNS-140, HTNS-450, respectively), using CSs in different particle sizes as templates. (d, g and j) TEM images of corresponding HTNSs (HTNS-40, HTNS-140, HTNS-450, respectively), using CSs in different particle sizes as templates. (k) Typical XRD patterns of HTNSs synthesized with CSs as templates. Inset shows typical XRD patterns of CSs/TiO_2 core-shell structures. The scale bar in (b to g) is 100 nm, (h and i) is 1 um, (j) is 500 nm, respectively.

(300–500 nm in diameter) were obtained (Fig. S7). This indicates the importance of size controlled CSs as templates for the synthesis of hollow structure in tunable diameters, which can be further evidenced by the TEM images shown in Fig. 3d, g, j. It should be noted that, with the mass ratio of CSs and TBOT kept consistent, the CSs with smaller size will template the synthesis of HTNSs with thinner shells (Fig. 3d, g, j). The shell thickness of HTNS-40 is even less than 5 nm, which is far less than the particle size of P25 (27 nm). It should be also noted that this calcination process could not only remove the CSs, but also increase the crystallinity of the obtained anatase HTNSs, as supported by the XRD patterns in Fig. 3k. The XRD pattern of the CSs/TiO_2 core-shell structure (inset pattern, Fig. 3k) shows no peaks indicative of the amorphous features, whereas after calcination the obtained HTNSs exhibit sharp and intense diffraction peaks well indexed to anatase TiO_2.

As well known that the SPV response starts to rise as soon as the photogenerated electrons and holes are separated in a photoexcited semiconductor, SPV spectra have been widely used to monitor the photogenerated charge separation in semiconductor photocatalysts [34].

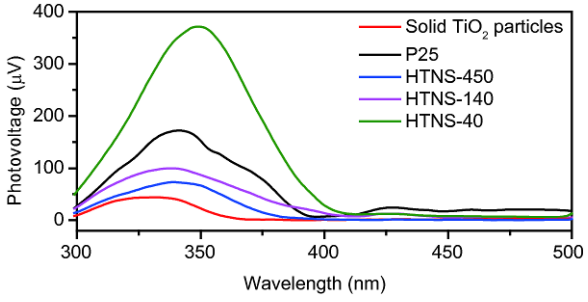

Figure 4 SPV of different structure of photocatalysts.

Fig. 4 shows the SPV spectra of HTNSs in different sizes, solid TiO_2 particles and P25. It can be seen that an obvious positive photovoltage response in the range of 300–400 nm for all the TiO_2 samples, which is the typical feature of an n-type semiconductor. The photovoltage response intensity increases as the particle size of HTNSs becomes smaller, and the HTNS-40 has the highest photovoltage response intensity, which is about twice that of P25. As expected, the solid TiO_2 particles have the lowest response intensity. It has been well accepted that the stronger the photoelectric signal, the higher the

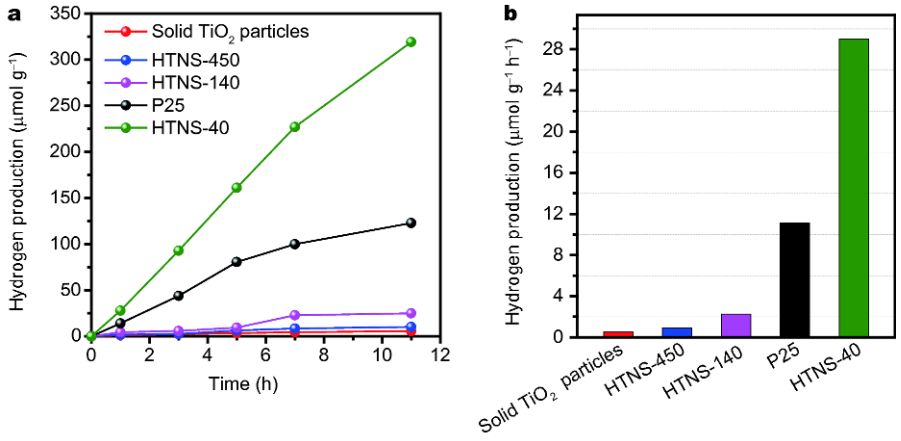

Figure 5 Photocatalytic performances of HTNSs in different sizes, solid TiO_2 nanoparticles and P25. (a) Time courses of photocatalytic hydrogen production, (b) photocatalytic hydrogen production rates.

charge separation efficiency [35]. That is to say, the separation efficiency of photogenerated electron-hole pairs can be effectively promoted in these HTNSs samples with thin shell structures; especially for HTNS-40 with the shell thickness of < 5 nm, the charge recombination could be effectively inhibited, due to the greatly shortened distance for charge carriers to transport to the surface, thus improving the charge separation efficiency [35–38].

Given the hollow structures benefiting photocatalysis [35], these obtained HTNSs were investigated for their superiority in photocatalytic hydrogen production in aqueous solution containing TEA as sacrificial reagent. Without photocatalyst or irradiation, no hydrogen was produced. Note that solid TiO_2 particles show negligible photocatalytic activity for hydrogen production without any co-catalyst, as shown in Fig. 5. In comparison, all the three HTNSs samples in different sizes demonstrate significant improvement in the photocatalytic activity for hydrogen production. The great increase in photocatalytic activities for the HTNSs samples should be related to the promoted charge transport and separation ability in the hollow structures with thin shell, which could be reasonably explained by the SPV. Moreover, the photocatalytic activities increase as the sizes of HTNSs decrease, and the highest hydrogen production rate of 30 μmol g_{cat}^{-1} h^{-1} is achieved over HTNS-40, which is about 64 and 3 times as high as that of solid TiO_2 and P25, respectively. The highest photocatalytic activity of HTNS-40 corresponds well with its highest signal in SPV spectra, indicating that the hollow structure with thin shell could ensure efficient photocatalysis. Another considerable reason for the high photocatalytic activity of HTNSs in smaller size (e.g., HTNS-40), as compared to HTNSs in larger sizes (e.g., HTNS-140 and HTNS-450) as well as solid TiO_2 particles and P25 is the larger specific area and more active sites of the hollow structures, which enable the effective contact between the catalyst and the solution in photocatalytic reactions [35,36].

CONCLUSIONS

In summary, CSs with diameter smaller than 100 nm were synthesized by a green and catalyst-free hydrothermal carbonization method for the first time. By varying the reaction parameters including initial pH values, glucose concentrations, reaction time and temperature, the sizes of CSs can be tuned from 450 nm to even 40 nm. Using the CSs as templates, size-controlled HTNSs were successfully prepared and then employed as photocatalysts for efficient hydrogen generation even without any co-catalyst. It was demonstrated that the photocatalytic activity could be significantly improved by HTNSs, as compared to solid TiO_2 and commercial P25; moreover, higher photoactivities were achieved with HTNSs with smaller sizes. Such photocatalytic enhancement achieved by the hollow structure with thin shell can be attributed to the greatly shortened distance for photogenerated charge carriers to the surface, leading to the improved charge separation efficiency, as well as the large specific area and enough active sites ensuring effective catalyst/solution contact and photocatalytic reactions. This study demonstrated an alternative and green approach for the facile synthesis of CSs with large-scale tunable diameters, and their application as templates for the further synthesis of hollow structures with thin shells for the potential utilization in different fields, such as catalysis, solar cells and energy storage devices, etc.

Received 7 November 2017; accepted 15 December 2017; published online 17 January 2018

1 O'Regan B, Graetzel M. A low-cost, high-efficiency solar cell based on dye-sensitized colloidal TiO_2 films. Nature, 1991, 353: 737–740
2 Chen X, Mao S. Titanium dioxide nanomaterials: synthesis, properties, modifications, and applications. Chem Rev, 2007, 107: 2891–2959
3 Wang B, Shen S, Mao S. Black TiO_2 for solar hydrogen conversion. J Materiomics, 2017, 3: 96–111
4 Cong H, Zhang M, Chen Y, *et al.* Highly selective CO_2 capture by nitrogen enriched porous carbons. Carbon, 2015, 92: 297–304
5 Jiang Z, Wei W, Mao D, *et al.* Silver-loaded nitrogen-doped yolk–shell mesoporous TiO_2 hollow microspheres with enhanced visible light photocatalytic activity. Nanoscale, 2015, 7: 784–797
6 Zhang Y, Zhao Z, Chen J, *et al.* C-doped hollow TiO_2 spheres: in situ synthesis, controlled shell thickness, and superior visible-light photocatalytic activity. Appl Catal B-Environ, 2015, 165: 715–722
7 Liu Y, Shen S, Ren F, *et al.* Fabrication of porous TiO_2 nanorod array photoelectrodes with enhanced photoelectrochemical water splitting by helium ion implantation. Nanoscale, 2016, 8: 10642–10648
8 Zhong Z, Yin Y, Gates B, *et al.* Preparation of mesoscale hollow spheres of TiO_2 and SnO_2 by templating against crystalline arrays of polystyrene beads. Adv Mater, 2000, 12: 206–209
9 Yang H, Zeng H. Preparation of hollow anatase TiO_2 nanospheres *via* ostwald ripening. J Phys Chem B, 2004, 108: 3492–3495
10 Chen X, Shen S, Guo L, *et al.* Semiconductor-based photocatalytic hydrogen generation. Chem Rev, 2010, 110: 6503–6570
11 Wang M, Pyeon M, Gönüllü Y, *et al.* Constructing Fe_2O_3/TiO_2 core–shell photoelectrodes for efficient photoelectrochemical water splitting. Nanoscale, 2015, 7: 10094–10100
12 Hulteen J, Martin C. A general template-based method for the preparation of nanomaterials. J Mater Chem, 1997, 7: 1075–1087
13 Gao A, Xu W, Ponce de León Y, *et al.* Controllable fabrication of Au nanocups by confined-space thermal dewetting for OCT imaging. Adv Mater, 2017, 29: 1701070
14 Joo J, Zhang Q, Dahl M, *et al.* Synthesis, crystallinity control, and photocatalysis of nanostructured titanium dioxide shells. J Mater Res, 2013, 28: 362–368
15 Gao M, Zhu L, Ong W, *et al.* Structural design of TiO_2-based photocatalyst for H_2 production and degradation applications. Catal Sci Technol, 2015, 5: 4703–4726
16 Rahman M, Tajabadi F, Shooshtari L, *et al.* Nanoparticulate hollow TiO_2 fibers as light scatterers in dye-sensitized solar cells: layer-by-layer self-assembly parameters and mechanism. ChemPhysChem, 2011, 12: 966–973
17 Rosseler O, Shankar M, Du M, *et al.* Solar light photocatalytic hydrogen production from water over Pt and Au/TiO_2 (anatase/rutile) photocatalysts: Influence of noble metal and porogen promotion. J Catal, 2010, 269: 179–190
18 Li A, Zhang P, Chang X, *et al.* Gold nanorod@TiO_2 yolk-shell nanostructures for visible-light-driven photocatalytic oxidation of benzyl alcohol. Small, 2015, 11: 1892–1899
19 Lyu F, Bai Y, Li Z, *et al.* Self-templated fabrication of CoO-MoO_2 nanocages for enhanced oxygen evolution. Adv Funct Mater, 2017, 27: 1702324
20 Yao C, Shin Y, Wang L, *et al.* Hydrothermal dehydration of aqueous fructose solutions in a closed system. J Phys Chem C, 2007, 111: 15141–15145
21 Li S, Pasc A, Fierro V, *et al.* Hollow carbon spheres, synthesis and applications–a review. J Mater Chem A, 2016, 4: 12686–12713
22 Cai T, Xing W, Liu Z, *et al.* Superhigh-rate capacitive performance of heteroatoms-doped double shell hollow carbon spheres. Carbon, 2015, 86: 235–244
23 Hu B, Wang K, Wu L, *et al.* Engineering carbon materials from the hydrothermal carbonization process of biomass. Adv Mater, 2010, 22: 813–828
24 Li X, Chen F, Lu X, *et al.* Layer-by-layer synthesis of hollow spherical CeO_2 templated by carbon spheres. J Porous Mater, 2010, 17: 297–303
25 Sun X, Liu J, Li Y. Use of carbonaceous polysaccharide microspheres as templates for fabricating metal oxide hollow spheres. Chem Eur J, 2006, 12: 2039–2047
26 Titirici M, Antonietti M. Chemistry and materials options of sustainable carbon materials made by hydrothermal carbonization. Chem Soc Rev, 2010, 39: 103–116
27 Zhang Y, Yang W, Luo R, *et al.* Preparation of carbon nanospheres by non-catalytic chemical vapor deposition and their formation mechanism. New Carbon Mater, 2016, 31: 467–474
28 Zhao X, Li W, Zhang S, *et al.* Facile fabrication of hollow and honeycomb-like carbon spheres from liquefied larch sawdust *via* ultrasonic spray pyrolysis. Mater Lett, 2015, 157: 135–138
29 Gong J, Liu J, Chen X, *et al.* Synthesis, characterization and growth mechanism of mesoporous hollow carbon nanospheres by catalytic carbonization of polystyrene. Micropor Mesopor Mater, 2013, 176: 31–40
30 Wang Q, Li H, Chen L, *et al.* Monodispersed hard carbon spherules with uniform nanopores. Carbon, 2001, 39: 2211–2214
31 Li Y, Li T, Yao M, *et al.* Metal-free nitrogen-doped hollow carbon spheres synthesized by thermal treatment of poly(*o*-phenylenediamine) for oxygen reduction reaction in direct methanol fuel cell applications. J Mater Chem, 2012, 22: 10911–10917
32 Xu D, Bu Q, Wang D, *et al.* Enhanced photoelectrochemical water oxidation performance by altering the interfacial charge transfer path. Inorg Chem Front, 2017, 4: 1296–1303
33 Sun X, Li Y. Colloidal carbon spheres and their core/shell structures with noble-metal nanoparticles. Angew Chem Int Ed, 2004, 43: 597–601
34 Funke A, Ziegler F. Hydrothermal carbonization of biomass: a summary and discussion of chemical mechanisms for process engineering. Biofuels Bioprod Bioref, 2010, 4: 160–177
35 Crossland E, Noel N, Sivaram V, *et al.* Mesoporous TiO_2 single crystals delivering enhanced mobility and optoelectronic device performance. Nature, 2013, 495: 215–219
36 Boury B, Plumejeau S. Metal oxides and polysaccharides: an efficient hybrid association for materials chemistry. Green Chem, 2015, 17: 72–88
37 Hu C, Xu Y, Duo S, *et al.* Preparation of inorganic hollow spheres based on different methods. Jnl Chin Chem Soc, 2010, 57: 1091–1098
38 Niu F, Shen S, Guo L. A noble-metal-free artificial photosynthesis system with TiO_2 as electron relay for efficient photocatalytic hydrogen evolution. J Catal, 2016, 344: 141–147

Acknowledgements The work was supported by the National Natural Science Foundation of China (51672210, 51323011 and 51236007), and the Natural Science Foundation of Shaanxi Province (2014KW07-02). Shen S was supported by the Foundation for the Author of National Excellent Doctoral Dissertation of China (201335), the National Pro-

gram for Support of Top-notch Young Professionals and the "Fundamental Research Funds for the Central Universities".

Author contributions Shen S and Feng X conceived the idea and supervised the project. Tan Y carried out the sample synthesis, characterizations and photocatalysis measurements. Wei D operated the SPV. Tang H conducted the TGA tests. Tan Y, Liu M and Shen S wrote the paper. All the authors discussed the results and revised the manuscript.

Conflict of interest The authors declare no conflict of interest.

Supplementary information Supporting data are available in the online version of the paper.

Yubo Tan is currently a PhD student of IRCRE, State Key Laboratory of Multiphase Flow in Power Engineering, School of Energy & Power Engineering, Xi'an Jiaotong University. Her research interests focus on nanoparticles for photocatalytic water splitting. From Oct. 2017 to Sept. 2019, she is a visiting scholar at the University of California, Riverside, USA, under the supervision of Prof. Yadong Yin for 2 years awarded by the China Scholarship Council (CSC).

Xinjian Feng received his PhD at the Institute of Chemistry, Chinese Academy of Sciences in 2006, and then he continued his scientific research at the University of Erlangen Nurnberg in Germany (2006–2007), Pennsylvania State University (2007–2012) and Chinese Academy of Sciences (2012–2015). In 2011, he was selected as the member in the first batch of "the Thousand Talents Plan" of the Central Organization Department. His research focuses on the designation and preparation of the electrode material and micro-nano structure; the transmission performance of electron and material in the surface and inside of electrode; the electrode materials in solar conversion and biosensing devices. So far, nearly 50 academic papers and research reviews have been published, including *Angew. Chem. Int. Ed.*, *Nano Lett.*, *Adv. Mater.*, *J. Am. Chem. Soc.*, etc. with more than 5,000 citations.

Shaohua Shen received his PhD at Xi'an Jiaotong University in 2010, and then he continued his postdoctoral at the University of California at Berkeley from November, 2011 to October, 2012. He is currently a full professor of IRCRE, the State Key Laboratory of Multiphase Flow in Power Engineering, School of Energy & Power Engineering, Xi'an Jiaotong University. He was the winner of the National Excellent Doctoral Dissertation, 2012. He has published more than 80 papers in *Chem. Rev.*, *Adv. Mater.*, *Nature Photon.*, etc., and received more than 6,800 citations. His research interests include the synthesis of nanomaterials and development of devices for photocatalytic and photoelectrochemical solar energy conversion.

直径小于100 nm空心二氧化钛纳米球的简单绿色可控合成及其光催化产氢性能研究

谭余波[1], 刘茂昌[1], 魏代星[1], 唐鹤鸣[2], 封心建[2*], 沈少华[1*]

摘要 碳球(CSs)因其在生物诊断、光子带隙晶体及药物输送等方面的广泛应用而成为该领域的研究热点, 而这些应用与碳球自身的形貌及尺寸息息相关. 在此, 我们实现了无任何催化剂及表面活性剂的情况下, 以葡萄糖为前驱体, 通过水热法成功制备形貌规整的碳球. 同时, 通过控制葡萄糖的浓度、反应时间和温度, 实现碳球尺寸在40–450 nm的可控调节. 进一步地我们以不同粒径的碳球为模板, 通过溶胶-凝胶法合成了不同粒径的中空二氧化钛纳米球(HTNSs), 并以其为催化剂进行光催化产氢实验. 结果表明, HTNSs的光催化活性与粒径有着紧密联系, 随着粒径的减小, 光催化活性得到显著增强. 同时, 不同尺寸HTNSs的光催化活性都远高于同样方法合成的实心二氧化钛纳米颗粒, 尤其是直径为40 nm的HTNSs的产氢量, 分别达到了实心二氧化钛颗粒及商业P25的64倍和3倍.

